Journal of Theoretical and Applied Vibration and Acoustics 6 (2) 388-409 (2020)

I S A V

Journal of Theoretical and Applied Vibration and Acoustics

journal homepage: http://tava.isav.ir

Investigation of reducing road-induced loads on sensitive payloads carried by road vehicles using a secondary suspension system containing double-ended magnetorheological dampers

Seyed Samad Samadani Agdam, Kamal Jahani*, Mohammad Reza Shabgard

[a]*Faculty of Mechanical Engineering, University of Tabriz, Tabriz, Iran*

ARTICLE INFO

Article history:
Received 14 February 2020

Received in revised form
5 June 2020

Accepted 5 October June 2020

Available online14 Novomber 2020

Keywords:
Secondary suspension system,

Magnetorheological damper,

Double-ended damper,

Sensitive-payload,

Road Vehicle.

ABSTRACT

Usually, payloads are carried on long routes with different road surface conditions and road obstacles by commercial vehicles from factory to destination. These road conditions cause trucks and their cargo to be exposed to shock and vibration of different amplitudes and frequencies that may impose catastrophic damages to delicate sensitive payloads. The aim of this paper is to present a 3-D model of a secondary suspension system, including double-ended magnetorheological dampers in cargo vehicles to protect sensitive cargo against induced excitations due to various road surface roughness. For this purpose, a double-ended magnetorheological damper for acquiring the desired minimum load capacity in an off-state situation and its maximum capacity when feeding 2Amp electric current was modeled, fabricated, and dynamically tested. Functional tests with sinusoidal harmonic inputs at different frequencies were performed using a UTM test machine and applying different electric currents to the damper. Considering these tests results, the parameters of the modified Bouc-Wen model for the damper are identified. Using the updated model for the damper, a 3-D model of the secondary suspension system with four magnetorheological dampers in the four corners of the cargo holder pallet is provided. The impact of the secondary suspension against the loads imposed by three types of road surface profiles, namely the road surface with the long harmonic wave, the bumpy road surface and the road surface with random roughness, is investigated. Furthermore, the effect of various uneven cargo mass arrangements on the magnitude of the dynamic loads of the payload is investigated. The results show that with increasing electric current at different road profiles, the vertical displacement amplitude has an average decrease of 40% in peak and 30% decrease in RMS, and at the same time, the isolation region has acceptable characteristics. These results indicate the proper performance of the proposed secondary suspension system in reducing the dynamic load level in sensitive payloads.

* Corresponding author:
E-mail address: ka_jahani@tabrizu.ac.ir (K. Jahani)

http://dx.doi.org/10.22064/tava.2021.138811.1174

1. Introduction

There are usually long routes for a truck to carry cargo from origin to destination and require crossing various roads. These routes include various types of roads such as highways, public roads, and even shoal roads with natural tolls such as downhill, uphill, turns, speed bumps, and various types of road surface quality conditions that cause trucks and their cargo to be exposed to shock and vibration of different amplitudes and frequencies. According to studies, the vibrations of freight vehicles are 9 to 16 times higher than those of passenger cars [1]. Also, on a ground ambulance, sick or injured patients as vibration-sensitive passengers in acute physical and skeletal conditions, brain injuries and heart problems are usually sensitive to even minor shocks and vibrations. Therefore, utilizing a proper suspension system plays a key role in isolating the vibrations of the vehicle body, occupants, and cargoes sensitive to road surface roughness and shocks. Adding to isolating road-induced excitations, isolation of vehicle body from powertrain excitations are also important in road vehicles [2].

In commercial vehicles such as trucks and Lorries, the two most important areas that are subjected to sudden high-amplitude shock and roadside vibrations are the driver's cab and the cargo deck, which are on the secondary suspension and the primary suspension of the vehicle, respectively [3]. Zhao et al. [4] proposed a seat-cab coupled system model and identified its parameters using simulation and test. Kim at el. [5] investigated using magnetorheological (MR) fluid-based mount for vibration control of a wheel loader cabin. Van Deusen [6] showed that by optimizing the truck's suspension, the quality of driving comfort would be greatly improved by reducing the stiffness of the suspension system in road surface vibrations.

Nowadays, reducing road-induced vibrations using semi-active suspension systems have increased considerably. The main advantage of this type of suspension system over passive suspension systems is its controllability and its need for small power sources and less expensive hardware compared to active suspensions [7]. Fischer et al. [8] reported that a semi-active and active suspension system could reduce vibration amplitudes by 20 to 30% and more than 30%, respectively. Marcu [9] tested a truck with a semi-active magnetorheological suspension system, including a controllable shock absorber for the driver's cab. The results showed improved vehicle comfort, steering ability, and reduced vibration amplitude. With the aim of reducing the transmission of vibrations and shocks of the road to an injured person and improving treatment conditions while transporting the patient in an ambulance, Chai et al. [10] proposed a model of a rigid plate instead of a stretcher and a medical chair as a secondary suspension with a double-ended magnetorheological damper.

Depending on the application, damping capacity, and location of installation, there are three primary types of magnetorheological dampers: single-tube, double-tube, and double-ended (two movable heads). By varying the type and size of the fluid passage, resizing and location of the coils, various models with different damping capacities are usually designed [11-15]. Desai et al. [16] developed and studied a twin-tube MR damper based on the damping values of a passive damper used in a passenger van. Xu and colleagues [17] designed and tested large-dimensional double-ended dampers with five electric coils to investigate the maximum amplitude of the damping force and the energy dissipation capacity by varying the number of active coils. The results of this study showed the significant effect of increasing the damper energy dissipation capacity and damping force by adding active coils and increasing external electrical current.

To identify the behavior of a magnetorheological damper and to use it for maximum efficiency and control in a semi-active system, there are developed mathematical models called parametric and nonparametric models [18]. The prediction accuracy, simplicity of equations, reliability, and compatibility are the most important criteria used to select an appropriate model. Dynamic parametric models include a set of linear and nonlinear viscous elements and linear and nonlinear springs. The parameters of the updated damper model are used to predict and control the behavior of vibrating systems consisting of several magnetorheological dampers in different operating conditions. To this end, constant and variable parameters with electric current intensity for these models are identified at each excitation frequency by comparing the dynamic responses of the mathematical model and the experimental counterpart using appropriate optimization techniques and algorithms [11, 19-21]. Spencer et al. [22] attempted to develop a new dynamic parametric model to estimate the inherent nonlinear intrinsic behavior of the damper. By improving the Bouc-Wen model by adding a mechanical element and a nonlinear viscous element, they presented the modified Bouc-Wen model. This model had high accuracy in reducing the error between experimental data and simulation on the load-speed hysteresis loops graph, specially in low-speed regions.

To ensure the permissible level of vibration amplitude and shock to sensitive cargoes, precautions should be taken to prevent high acceleration or displacement of sensitive cargoes. Different techniques can be chosen in this regard. One solution could use either an active or semi-active suspension system in the vehicle's primary suspension or to use a secondary suspension system on the cargo floor with controllable suspension elements. The other solution could be using appropriate packaging for the payload with enough shock and vibration isolation capability for the package that can increase the overall price of the payload.

Usually, the load arrangement is not uniform across the freight segment and varies depending on the type of load or loading and unloading along the route.

According to the literature, even though there are intensive published works to protect the cabin and crew of trucks using secondary suspension systems [9, 23-25], however, using this idea for protecting the sensitive payload has not been reported yet and also a limited number of works can be found in the literature main objective of this paper is to investigate the concept of using a secondary suspension system, including magnetorheological dampers in cargo vehicles to reduce the transmitted loads to sensitive cargo against induced excitations due to various road surface roughness

In this paper, to reduce the vibration amplitude of the sensitive cargo in a truck, first, a suitable double-ended magnetorheological damper is designed based on the calculation of fluid pressure drops inside the damper ducts in the presence of a magnetic field to provide minimum and maximum desired force capacities. Then, dynamic tests are conducted with harmonic inputs on the fabricated prototype damper. By applying the dynamic test results and estimating the parameters of the modified Bouc-Wen model, the electric current dependent parameters are defined as polynomial and exponential functions through curve fitting. Then, the 3D vibrational model of the truck, including a secondary magnetorheological suspension system, with an irregular layout of the sensitive payload, is developed. Finally, in order to investigate the effect of the change in the mass of the sensitive cargo on the vibrational amplitude of the cargo as well as the effect of the change of feeding electric current to the magnetorheological damper on the

performance of the secondary suspension system while considering different road surface irregularities, the derived equations are solved and obtained results discussed.

2. Designing, Fabricating, and testing a double-ended MR damper

A schematic diagram of the circular duct double-ended magnetorheological damper designed in this study is presented in Fig.1. The damper is divided by the piston into two parts, the upper and lower chambers, which are filled with magnetorheological fluid and fluid moves between the two chambers in each movement cycle of the magnetorheological damper. As the fluid passes through the circular duct at a distance d_c from the cylinder, the variable external magnetic field affects the fluid and disperses the dispersed particles of the iron powder in magnetorheological fluid based on the direction of the magnetic field in a chain arrangement. At this point, the fluid undergoes shear strain and changes from a Newtonian fluid to a non-Newtonian fluid. This process is amplified by increasing the magnetic field intensity and changing the viscosity of the fluid and returning to its original state by disconnecting the electric current from the fluid. Force capacity of this type of damper depends on the damper dimensions, characteristics of carrier fluid, magnetic behavior of iron particles, the type of metal used in the piston and cylinder, the number of coils, and their diameter [26].

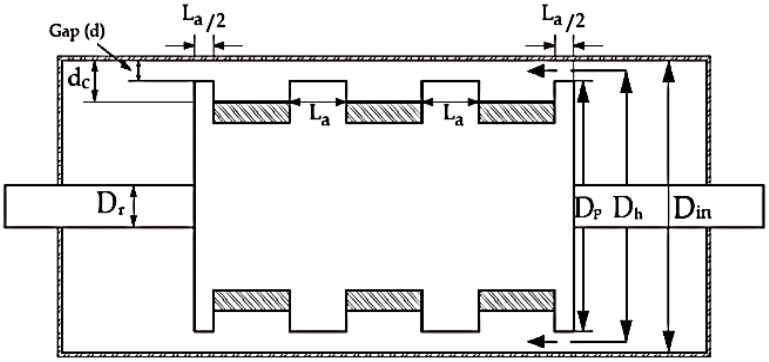

Fig 1: Schematics of double-ended MR damper with three electric coils

Since the distance between the cylinder and the piston is very small compared to the active length between the two coils, in the equations of force, the cylinder and piston can be considered as two parallel plates to each other with the fluid flow passing through them. The damping force is calculated from pressure drops within the duct. This force is written as the sum of the semi-active magnetorheological force that is a function of shear stress of the magnetorheological fluid and the passive force of the carrier fluid viscosity [27]:

$$F_D = (F_{MR} + F_V) sgn(V_P) \tag{1}$$

where, F_{MR} for the three electric coils is produced by shear stress that is obtained according to Equations (2) and (3):

$$F_{MR} = nA_P \Delta P_{MR} \tag{2}$$

$$\Delta P_{MR} = \frac{2L_a \, \tau_{MR_y}}{d} \tag{3}$$

In these equations, F_{MR} is the damping force due to the magnetic field when feeding the coils with electric current, F_V is the Off-state viscous force, n is the number of electric coils and τ_{MR_y} for shear stress and is a function of the magnetic field intensity.

A quadratic polynomial is used to describe the relationship between yield stress and magnetic introduction [28].

$$\tau_{y\,MR} = \alpha_1 B^2 + \alpha_2 B + \alpha_3 \tag{4}$$

The initial values for coefficients of Eqn. 4 is considered as follows:

$\alpha_1=1.43\times10^{-6}$, $\alpha_2=4.74\times10^{-4}$ and $\alpha_3= -1$

These coefficients will be tuned after dynamic tests of the investigated damper. Based on Kirchhoff's laws, the magnetic induction, B, can be calculated as follows:

$$\oint Hdl = NI \cong \frac{2\,hB}{\mu} \tag{5}$$

$$B = \frac{\mu NI}{2\,h} \tag{6}$$

where μ is the magnetic permeability of the MR fluid, I is the input current to be applied to the MR damper; N is the number of turns of the coil and h is the width of the damping path.

The passive force of the damper is a combination of pressure drop along the channel, Δp_η, pressure drop caused by a partial fluid loss in the channel, Δp_{ml}, pressure drop during fluid passage through coil due to micro losses, Δp_{coil} ,the pressure drop due to magnetorheological fluid at entry and exit and Δp_E. These pressure drops are defined as follows [27, 29, 30]:

$$\Delta p_\eta = \frac{\rho}{2} {V_d}^2 \frac{f L_a}{2d} \tag{7}$$

$$\Delta p_{ml} = \frac{\rho}{2} {V_d}^2 (K_{SC} + K_{SE}) \tag{8}$$

$$\Delta p_{coil} = \frac{\rho}{2} {V_c}^2 \frac{f_c L_c}{2d_c} \tag{9}$$

$$\Delta p_E = \rho {V_d}^2 \left(K_{entry} + K_{exit}\right) \tag{10}$$

in which ρ is the density of the magnetorheological fluid, f is the Darcy friction coefficient inside the MR fluid passage, f_c Darcy friction factor inside the coil gap and V_d and d_c are the average velocities of fluid passing through the passage, and the distance between the coil and the magnetorheological damper cylinde,

$$V_d = \frac{A_p V_p}{A_d} = \frac{A_p V_p}{\pi\, D_b d} \quad ; \quad V_c = \frac{A_p V_p}{A_c} \tag{11}$$

where A_p , A_d and A_c are the areas of the piston, MR valve cross-section and coil gap cross-section, respectively; and V_p is the velocity of the piston.

Experimental coefficients $K_{SE}.K_{SC}.K_{entry}\ and\ K_{exit}$ represent the experimental coefficient of sudden expansion, the experimental coefficient of sudden contraction, the experimental coefficient of impact of the fluid inlet, and the experimental coefficient of impact of the fluid outflow, respectively, which are defined according to the following equations [27, 30].

$$K_{SE} = K_{exit} = \left(1 - \frac{A_d}{A_c}\right)^2 \quad ; \quad K_{SC} = K_{entry} = 0.42\left(1 - \frac{A_d}{A_c}\right) \tag{12}$$

Finally, the passive viscose force of the magnetorheological damper for the 3 electrical coils is written as Eqn. 13:

$$F_v = A_P\left[3\left(\Delta P_\eta + \Delta P_{ml} + \Delta P_{coil}\right) + \Delta P_E\right] \tag{13}$$

Appropriate material for actuation interfaces (piston and cylinder) in this kind of dampers must owe two main characteristics, namely having good wear resistance and being ferromagnetic. When a ferromagnetic material is selected for the actuation interfaces , with increasing the attractive magnetic force between the particle chains in the magnetorheological fluid and the interfaces, the yield stress value is increased [31]. Since CK45 electroplated steel has good wear resistance and is a ferromagnetic material, therefore it is selected for the piston and cylinder in this research. The geometrical characteristics of the damper are extracted and determined based on desired damping force of the magnetorheological damper for the minimum value ($3000N$ at zero Amp) and the maximum value ($6500N$ at the maximum tolerable electric current of 2 Amp).

To solve the Eqn. (13) and find, the hysteresis behavior of the MR damper, at first a sinusoidal displacement excitation with specific maximum displacement amplitude and frequency for the piston rod is considered. Then, by differentiating this assumed displacement-time signal, the corresponding velocity-time signal for the piston rod is attained. Consequently, using this velocity-time signal in Eqn. (13), the force-time signal for the damper is achieved. Finally, using these signals in each time step for a given time duration (for a specific number of oscillations), the force- velocity and force-displacement hysteresis loops for the damper are plotted.

The geometrical dimensions of the desired prototype for the damper that can produce the above-mentioned target damping forces based on the above-described simulation procedure are presented in Table 1. The obtained hysteresis curves from the simulation of (13) with harmonic displacement inputs with an oscillation frequency of 1 Hz and amplitude of ±15 mm at different electric current intensities are presented in Fig. (2a-2c). According to Fig 2-b, the force-velocity mostly has a linear trend and, in low velocities, shows hysteresis behavior that is in agreement with the results provided for this kind of damper in the literature [10, 14].

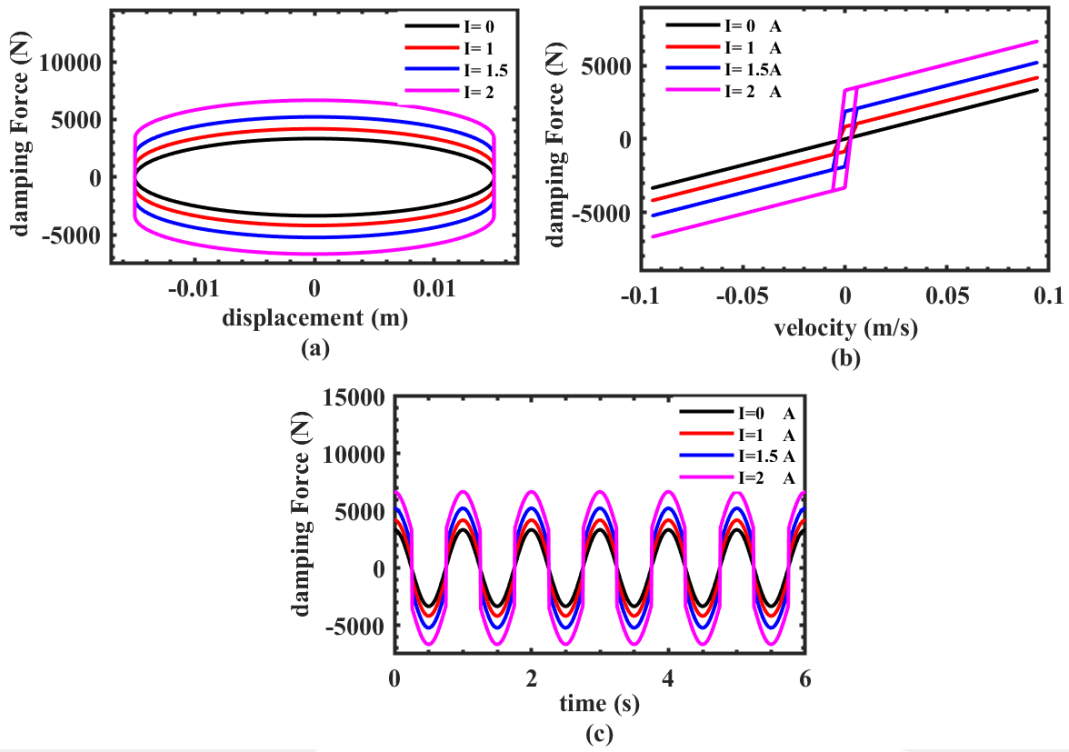

Fig 2: Predicted damping force of the MR Damper using nonlinear equations of active and passive force: (a) Damping force versus displacement (b) Damping force versus velocity (c) Damping force versus time.

Table 1: Geometrical characteristics of the double-ended Magnetorheological damper

Parameter	size
Inner diameter of hydraulic cylinder (D_{in})	$95mm$
MR circular valve thickness (d)	$1mm$
Number of electromagnetic coils (n)	3
piston diameter (D_p)	$93mm$
Coil length of a single stage (L_c)	$22mm$
Copper wire diameter for winding coils	$0.8mm$

For providing a magnetorheological fluid for the damper, according to studies in this field [26, 32-34], spherical carbonyl iron powder with a diameter of $40\mu m$ and density of $7.86\frac{g}{cm^3}$ and purity of 99.5%were used for the dispersed phase of the magnetorheological fluid with a volume percentage of 25%. Also, in the continuous phase, H-68 hydraulic oil base fluid with a viscosity of $68cSt$ at 40℃ and $9cSt$ at 100℃, with 67%volumetric percentage, with lithium-based high-pressure refractory grease additive, with 8% percentage volume was used to increase stability and prevent the formation of iron masses. The main advantage of the used particles in this study is that since it is used vastly in metallurgy powder industry and consequently has considerably low price and are more available compared to the smaller in diameter and more expensive

particles reported in the literature. On the other hand, the results of sedimentary tests show that its sedimentation rate is acceptable (Fig. 3) for using in dampers that are usually in movement in dynamic systems such as automotive shock and vibration isolators.

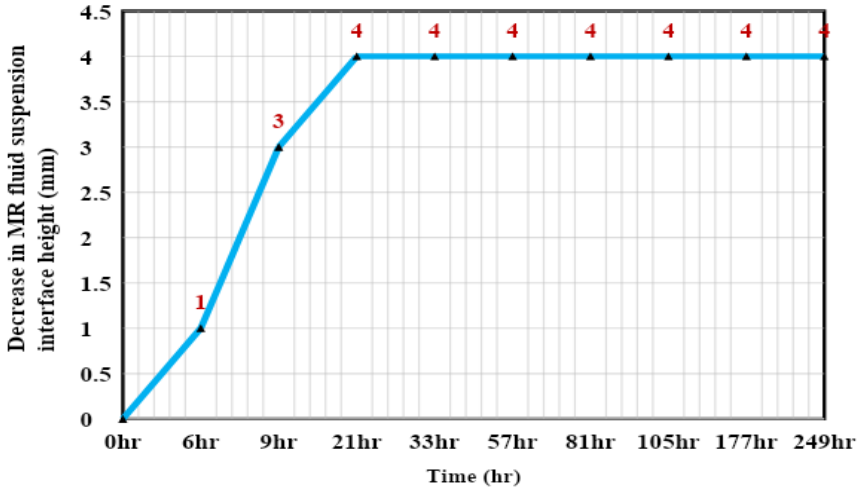

Fig 3: Magnetorheological fluid sedimentation graph, in the range of 250 hours at room temperature

The laboratory test suite shown in Fig. 4 includes a Zweik Roell Amsler HA 250 Dynamic Hydraulic Testing Machine equipped with a load cell, displacement measurement sensor, hydraulic control unit, Workshop96 software for recording data and a controllable electric current supplier. The sinusoidal harmonic excitation is applied to the damper. The maximum damper stroke in all tests is $\pm 15mm$, the excitation frequencies are $0.25Hz$, $0.5Hz$. The electric currents applied to the damper at each frequency of excitation are 0, 0.5, 1, 1.5 and 2 Amps.

As a sample from the conducted tests, Fig. 5 shows the experimental results of the magnetorheological damper test at 0.5 Hz excitation frequency and different electric currents. Table 2 shows the ratio of the maximum damping force amplitude of the magnetorheological damper in different electrical currents to the maximum damping force amplitude at the off-state situation (zero-ampere electrical current). This ratio, hereinafter, is called the dynamic range. The results show that with increasing electric current, the dynamic range increases considerably, which confirms the acceptable performance of the manufactured prototype of the MR damper. Also, from Fig. 5b it can be concluded that the maximum generated damping forces by the manufactured prototype damper are in agreement with theoretically predicted counterparts.

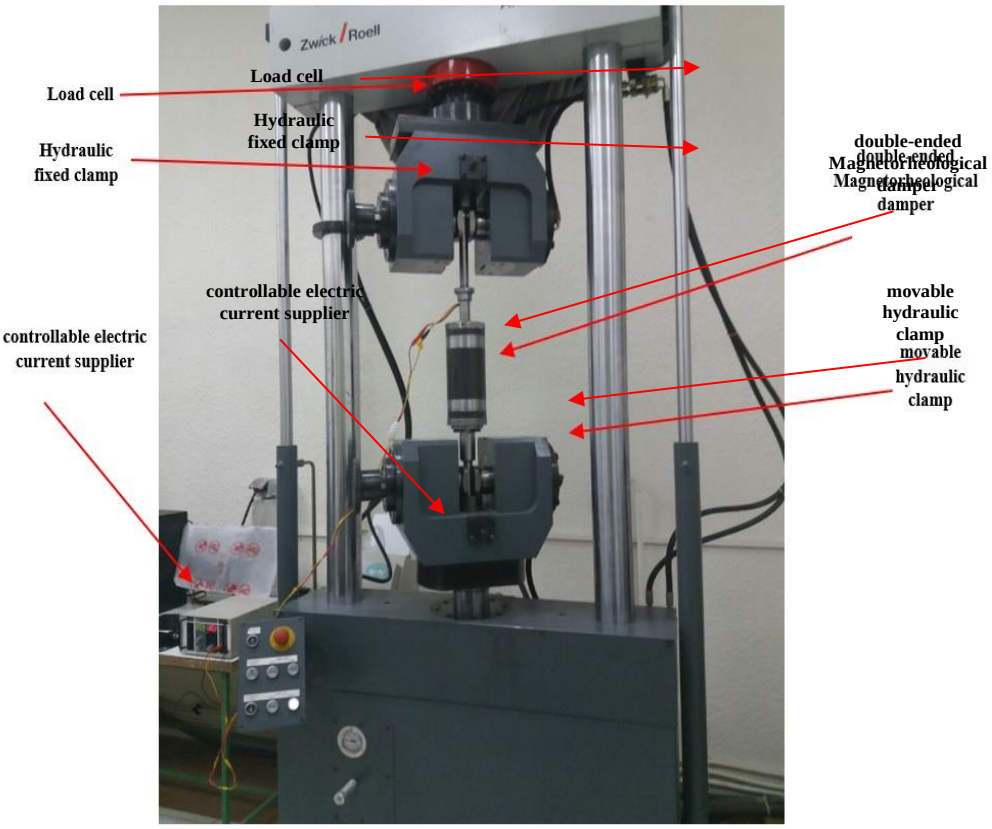

Fig 4: Experimental setup for testing MR Damper

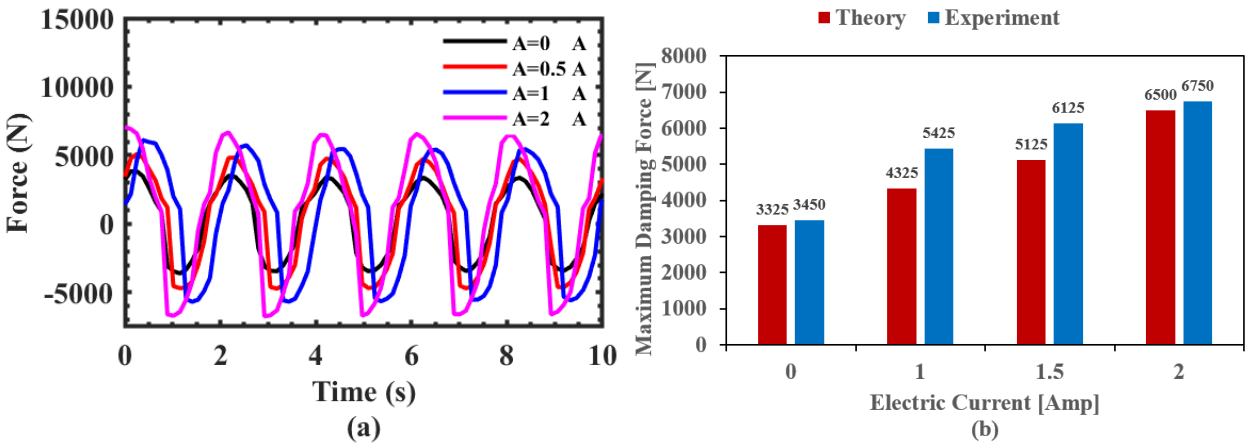

Fig5: Experimental characteristics of the investigated MR Damper in frequency 0.5Hz for MRF40µm: (a**)** Force-time and (b**)** Maximum damping force comparison between theory and experiment

Table 2: The dynamic range of the magnetorheological damper in different electrical currents

Electric current intensity (Amps)	Dynamic Range
0.5	1.414
1	1.620
1.5	1.802
2	1.920

3. Secondary suspension system including MR damper

The model presented in Fig. 6 is designed to provide a secure secondary magnetorheological suspension system for carrying a sensitive cargo by truck. In this model, on the chassis of the truck's primary suspension is a rigid rectangular plate as representative of a sensitive load pallet with the dimensions listed in Table 3. At the four corners of this rigid plate are magnetorheological dampers identical to the constructed and tested sample in section 2, parallel with linear coil springs.

In modeling, it is assumed that the sensitive cargo will be at the center of mass of this system (for balanced mass distribution, see section 4), such that the mass center displacements of the designed suspension system are the same as the displacements of the sensitive cargoes. The geometrical distances of this plate relative to the center of mass are shown by the longitudinal geometric parameters a_5 , a_6 and transverse parameters b_5 and b_6.

Since the chassis center of mass of the primary suspension system and the secondary suspension system are not concentric, the geometric parameters a_3, a_4, b_3 and b_4 are used to indicate the longitudinal and transverse distances of the pallet to the center of mass of the vehicle. In the model presented for the truck, the Y_1 and Y_2 excitation from the right and left sides of the vehicle are inserted from the road surface into four tires modeled with springs K_{r1}, K_{r2}, K_{l1}, K_{l2}, and masses m_{r1}, m_{r2}, m_{l1} ,m_{l2}.

The stiffness of the springs of the truck's primary suspension system along the vertical direction is obtained based on the amount of static displacement assumption that was chosen in the present study as the vertical displacement value of $2.5cm$ [35]. Then, the stiffnesses of the springs were determined based on the mass distribution and, consequently the gravitational force distribution on each part. The specifications of the considered sprung and unsprung masses for the sensitive cargo and the truck, springs stiffnesses and model dimensions are presented in Table 3. The values provided for different parameters in this table have been adapted from general specifications of a sample commercial light truck from the market [36], considering some of the parameters provided in the ref [35] and assuming an uneven mass distribution for the sensitive payload.

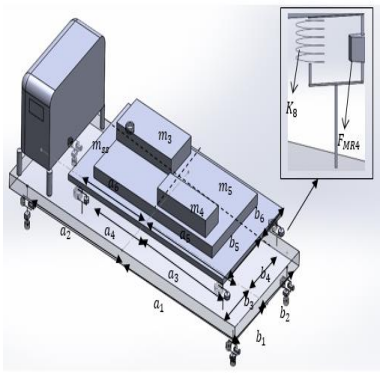

(a)

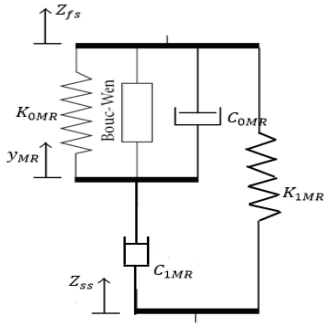

(b)

Fig6: (a) Schematic of a secondary suspension system with a magnetic magnetorheological damper in the sample truck whole model, (b**)** Modified Bouc-Wen (Spencer) parametric model for MR damper

Table 3: Geometric properties of the considered truck model

Parameters	Symbols	Value	Parameters	Symbol	Value
Chassis mass of secondary suspension system	m_{ss}	321 (kg)	Sprung mass Primary suspension	m_{fs}	1800kg
Tire stiffness	$K_{l1}.K_{l2}.K_{r1}.K_{r2}$	75000 $(\frac{N}{m})$	Unsprung mass Primary suspension	$m_{r1}.m_{r2}.m_{l1}.m_{l2}$	225kg
Main suspension stiffness	$K_1.K_2.K_3.K_4$	25000 $(\frac{N}{m})$	Sprung mass Secondary suspension	m_3	700kg
Secondary suspension stiffness	$K_5.K_6.K_7.K_8$	25000 $(\frac{N}{m})$	Sprung mass Secondary suspension	m_4	400kg
Distance of suspension from C.M	$a_1.a_6$	2.28 (m)	Sprung mass Secondary suspension	m_5	1200kg
Distance of suspension from C.M	$a_2.a_3.a_4$	1.52 (m)	Distance of suspension from C.M	a_5	0.76m
Distance of suspension	$b_3.b_4$	0.61 (m)	Distance of suspension from	$b_1.\ b_2$	0.82m

from C.M			C.M		
Distance of suspension from C.M	b_6	0.3 (m)	Distance of suspension from C.M	b_5	0.91m
Damping coefficient	$C_1.C_2.C_3.C_4$	1224.745 $(\frac{N.s}{m})$			

The model proposed for the truck, including the secondary magnetorheological suspension system, has a total of 10 degrees of freedom. The equations of motion of the whole system are made up of three interconnected parts, the first part (A) of tires and the axles with four degrees of freedom, the second part (B) of the main chassis over the primary suspension system with three degrees of freedom, and the third part (C) of a rigid rectangular plate as the chassis of the sensitive cargo pallet with irregular cargoes overlayed on the secondary suspension system with three degrees of freedom. The equations of motion of this model, based on the above classification by Newton's second law, are written as follows.

A:

$$m_{l1}\ddot{z}_{l1} = -K_{l1}z_{l1} + C_1\dot{Y}_{t1} + K_1Y_{t1} + K_{l1}Y_1 \quad (14)$$

$$m_{l2}\ddot{z}_{l2} = -K_{l2}z_{l2} + C_2\dot{Y}_{t2} + K_2Y_{t2} + K_{l2}Y_1 \quad (15)$$

$$m_{r1}\ddot{z}_{r1} = -K_{r1}z_{r1} + C_3\dot{Y}_{t3} + K_3Y_{t3} + K_{r1}Y_2 \quad (16)$$

$$m_{r2}\ddot{z}_{r2} = -K_{r2}z_{r2} + C_4\dot{Y}_{t4} + K_4Y_{t4} + K_{r2}Y_2 \quad (17)$$

B:

$$m_{fs}\ddot{z}_{fs} = -C_1\dot{Y}_{t1} - K_1Y_{t1} - C_2\dot{Y}_{t2} - K_2Y_{t2} - C_3\dot{Y}_{t3} - K_3Y_{t3} - C_4\dot{Y}_{t4} - K_4Y_{t4} + K_5Y_{P1} + K_6Y_{P2} + K_7Y_{P3} + K_8Y_{P4} - F_{MR1} - F_{MR2} - F_{MR3} - F_{MR4} \quad (18)$$

$$I_{x_{fs}}\ddot{\theta}_{fs} = -a_2\left(C_1\dot{Y}_{t1} + K_1Y_{t1}\right) + a_1\left(C_2\dot{Y}_{t2} + K_2Y_{t2}\right) - a_2\left(C_3\dot{Y}_{t3} + K_3Y_{t3}\right) + a_1\left(C_4\dot{Y}_{t4} + K_4Y_{t4}\right) + a_4(K_5Y_{P1}) - a_3(K_6Y_{P2}) + a_4(K_7Y_{P3} - a_3(K_8Y_{P4}) - a_4F_{MR1} + a_3F_{MR2} - a_4F_{MR3}) + a_3F_{MR4} \quad (19)$$

$$I_{x_{fs}}\ddot{\theta}_{fs} = b_2\left(C_1\dot{Y}_{t1} + K_1Y_{t1}\right) + b_2\left(C_2\dot{Y}_{t2} + K_2Y_{t2}\right) - b_1\left(C_3\dot{Y}_{t3} + K_3Y_{t3}\right) - b_1\left(C_4\dot{Y}_{t4} + K_4Y_{t4}\right) - b_4(K_5Y_{P1})) - b_4(K_6Y_{P2}) + b_3(K_7Y_{P3})) + b_3(K_8Y_{P4})) + b_4F_{MR1} + b_4F_{MR2} - b_3F_{MR3}) - b_3F_{MR4} \quad (20)$$

C:

$$(m_{ss} + m_3 + m_4 + m_5)\ddot{z}_{ss} = -K_5Y_{P1} - K_6Y_{P2} - K_7Y_{P3} - K_8Y_{P4} + F_{MR1} + F_{MR2} + F_{MR3} + F_{MR4} \quad (21)$$

$$I_{y_{ss}}\ddot{\theta}_{ss} = -a_6K_5Y_{P1} + a_5K_6Y_{P2} - a_6K_7Y_{P3} + a_5K_8Y_{P4} + a_6F_{MR1} - a_5F_{MR2} + a_6F_{MR3} - a_5F_{MR4} \quad (22)$$

$$I_{x_{ss}}\ddot{\varphi}_{ss} = b_6K_5Y_{P1} + b_6K_6Y_{P2} - b_5K_7Y_{P3} - b_5K_8Y_{P4} - b_6F_{MR1} - b_6F_{MR2} + b_5F_{MR3} + b_5F_{MR4} \quad (23)$$

where relations for $Y_{t1} - Y_{t4}$ and $Y_{P1} - Y_{P4}$ are presented The Appendix.

Here, the relation of the magnetorheological damper's damping force is derived based on Modified Bouc-Wen(Spencer) parametric model, which has high accuracy in estimating the experimental hysteresis curves. Since the damper is positioned between two rigid plates with vertical and rotational motions, so the Spencer model equations for one of the dampers will be as follows:

$$F_{MR1} = C_{1MR}\left(\dot{y}_{MR1} - \left(\dot{z}_{ss} + a_6\dot{\theta}_{ss} - b_6\dot{\varphi}_{ss}\right)\right) - K_{1MR}\left(Y_{P1} - z_{0_{MR1}}\right) \tag{24}$$

The complementary variable $\dot{y}_{MR1}$ in equation 24 is written as follows:

$$\dot{y}_{MR1} = \frac{1}{C_{0MR} + C_{1MR}}\left(-\alpha\dot{z}_{MR1} + C_{0MR}\dot{Y}_{m1}\right) + C_{1MR}\left(\dot{z}_{ss} + a_6\dot{\theta}_{ss} - b_6\dot{\varphi}_{ss}\right) + K_0(Y_{m1} - y_{MR1}) \tag{25}$$

The variable z in the above equation, which is used in expressing the hysteresis behavior of the Spencer model, is obtained by solving the following equation:

$$\dot{z}_{MR1} = -\gamma\left|\dot{y}_{MR1} - \dot{Y}_{m1}\right|z_{MR1}|z_{MR1}|^{n-1} - \beta\left|\dot{y}_{MR1} - \dot{Y}_{m1}\right||z_{MR1}|^n + A\left|\dot{y}_{MR1} - \dot{Y}_{m1}\right| \tag{26}$$

In order to investigate the impact of road profile type on the level of vibrations and shocks inflicted on sensitive cargo; this study considers three types of road profiles that are: sinusoidal harmonic road profiles, speed bump profiles and random profiles according to ISO8608 standard. The function of the sinusoidal harmonic profile considered as the input of the models in this research is as the relation of (27).

$$Y(t) = h(\sin\left(\omega\left(t - \frac{D_{car}}{\lambda}\right)\right)) \tag{27}$$

In the above relation, the frequency of the road profile is defined as $\omega = \frac{2\pi V}{\lambda}$, h is the amplitude of the sine wave, λ is the length of sine wave or wavelength and V is the vehicle speed.

The speed bump profile function in this study, is as equation (28). The time delay between the front and rear wheels in Equation (28), which is the ratio of the distance between the two axles of the truck to its speed, is deducted from the total time.

$$Y_{(t)} = \{h\ sin\ \sin\left(\omega(t - t_0)\right) \qquad t_0 \le t \le \frac{pi}{\omega}\ 0 \qquad otherwise \tag{28}$$

In designing an artificial road according to ISO standard, the road is considered as a harmonic function with white Gaussian noise, which by choosing the coefficient of the roughness of the road, ultimately governs the profile of random road irregularities based on classifications of ISO8608 is written as follows [37]:

$$Y(x) = \sum_{i=0}^{N}\sqrt{\Delta n}2^k 10^{-3}\left(\frac{n_0}{i\,\Delta n}\right)\cos(2\pi i\,\Delta n x + \vartheta) \tag{29}$$

Equation 29 is a function of the displacement of x, but is written as a function of time to simulate and apply it as a random road entry, for example, assuming a constant speed of $12\frac{m}{s}$ ($45\frac{km}{h}$). Assuming that the length of the simulated artificial road L is 125m, then the simulated duration

must be $10s$ to reach the assumed speed. Accordingly, $\Delta n = \frac{1}{L}$ and B is the sampling interval. The constant parameter k is defined by dividing the road profiles by integers from 3 to 9 for profiles A to H.

4. Results and discussions

4.1. Performance of the secondary suspension system under various road conditions

In this section, three types of road roughness are considered to evaluate the performance of the secondary suspension system containing double-ended magnetorheological dampers under different road roughness conditions. These selected road surface obstacles for further investigations are the most frequently experienced road roughness by commercial vehicles in carrying payloads through different roads: **a**) Smooth Road with a speed bump, **b)** Road with uniform harmonic wave roughness and **c)** Road with random surface roughness

4.1.1. smooth road with a speed bump

The intended speed bump is a sinusoidal half-wave obstacle with a height of 0.15m and a width of 1.2m which is assumed the vehicle hit it at a very low speed of $1.5\frac{m}{s}$ (approximately $5\frac{km}{h}$). Figs.7a and 7b show, respectively, the time and frequency responses in the vertical direction of the secondary magnetorheological suspension system at the payload center of mass with a total cargo mass of $2300Kg$. As can be seen in facing to speed bumps, as the electric current increases, the damping capacity of the damper increases, resulting in a large decrease in the vertical displacement amplitude. The vertical displacement has decreased from $0.16m$ (in the zero Amp electric current) to $0.091m$ (in $1.6\ Amp$ electric current), equivalent to 43% reduction in the displacement amplitude.

Figs. 7c – 7d show the time and frequency response of the secondary magnetorheological suspension system in relation to the pitch and roll angular displacements, respectively. As can be seen in Figs. 7c and 7d, the angular displacement amplitude of the pitch in the zero Amp electric current is changed relative to $1.6Amp$ electric current and decreases by $0.013rad$ at the peak of the curve, but after passing the system from the peak point, the results show that over the time, a current of 0.5 amperes is more effective in reducing amplitude than other electric currents.

4.1.2. Road with uniform wave roughness (harmonic roughness)

The road with uniform wave roughness in this study has a wavelength of $5m$ and a peak height of $0.1m$ and the vehicle is traveling at a relatively slow speed of $15\frac{km}{h}$ ($4\frac{m}{s}$). Fig. 8 shows the time and frequency response of the secondary magnetorheological suspension system at the vertical, pitch, and roll displacements in the center point of the payload with a total cargo mass of $2300kg$. As can be seen from this figure, by applying harmonic inputs in the truck model, the effect of increasing the electric current on the vertical, pitch and roll displacement are quite different, so that as seen from Figs. 8a and 8b, with increasing electric current from 0 Amp to $1.6Amp$, vertical displacement amplitude at peak point decreases by $0.053m$ and as the electric current increases, the vertical displacement amplitude decreases further. Also, by increasing the

electric current from 0 Amp to 1.6Amp the RMS of vertical displacement amplitude also results in a decrease of 0.033m(59%).

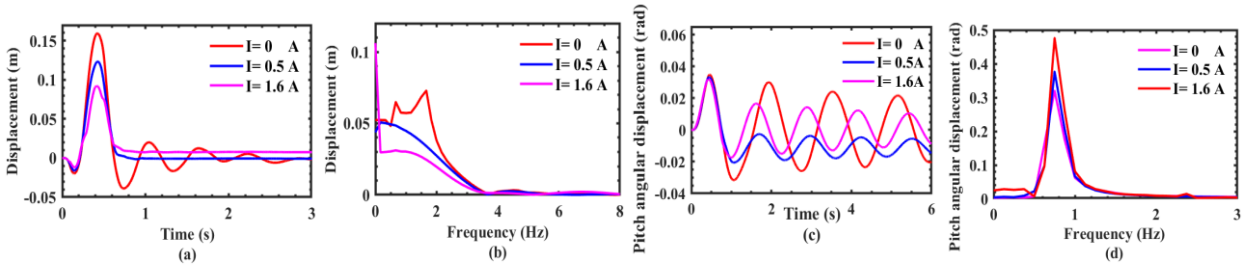

Fig 7: Time and frequency responses: (a), (b) Vertical displacement (c), (d) Pitch angle of center mass of payload with 2300kg mass for speed-bump profile

But according to Figs. 8c, 8d and Figs. 8e, 8f, which respectively show the pitch and roll angular responses for the harmonic input, their amplitudes, however, are different from the vertical displacement amplitudes. Comparing the peak points, the amplitude is increased 0.057rad when the applied electric current is 1.5 Amp comparing to the off-state (0 Amp) situation. The reason for this can be attributed to the same forces applied by the dampers to the four corners of the rigid plate overlaying on top of the secondary suspension system and the irregular mass layout, which both by increasing the electric current, amplify the pitch angle and roll angles.

4.1.3. Road with random surface roughness

Road surface with random roughness (k=7) according to ISO8608 standard is considered here and it is assumed that the vehicle is driven at a constant speed of 45km/h (12m/s). As can be seen in Fig. 9, the vertical and angular pitch amplitude decreases with increasing electric current like the results of the harmonic and speed bump inputs. So, the RMS value of the vertical displacement amplitude is reduced to 0.012m by changing the current from zero Amp to 1.6Amp. The RMS of the pitch angle of the center of mass of the secondary suspension is also reduced 2.5$e^{-4}rad$ equal to 59%, as expected, by a change of electric current from zero Amp to 1.6Amp. But the roll angle displacement of the secondary suspension model increases with the increase in electric current from zero Amp to 1.6Amp, which was also observed in the harmonic inputs, as well as the reasons for this.

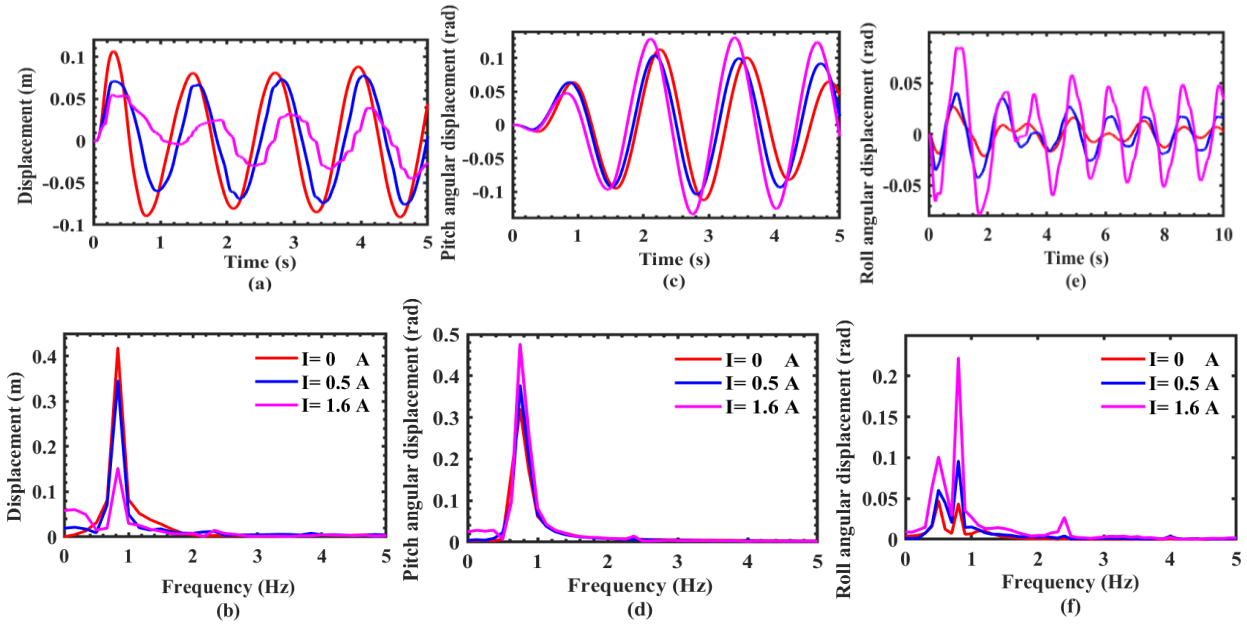

Fig 8: Time and frequency responses: (a), (b) Vertical displacement, (c), (d) Pitch Angle, (e), (f) Roll angle of center mass of payload with 2300kg mass for harmonic road roughness profile

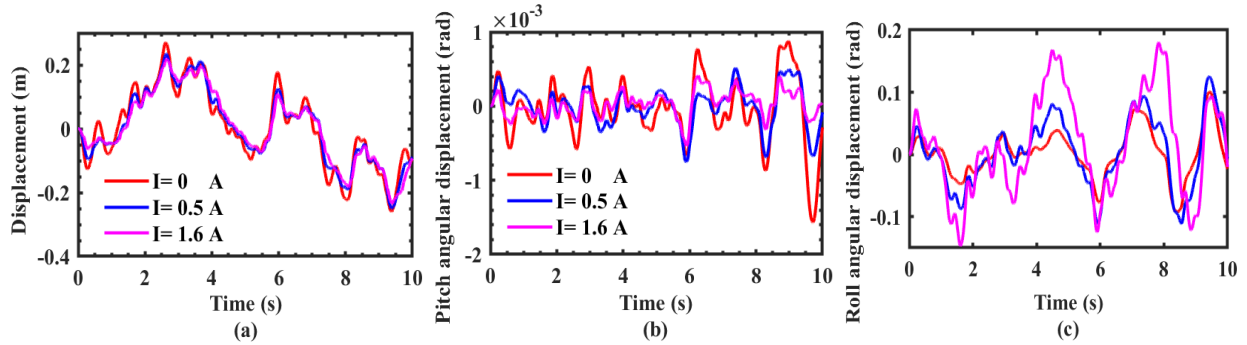

Fig 9: Time response of: (a) Vertical displacement, (b) pitch angle, and (c) roll angle for random profiles with coefficient k=7

In a general overview, from the simulation results of the proposed model, for the truck containing a secondary suspension system magnetorheological damper, on different road profiles, according to the results of Table 4, it is observed that, as the electric current increases, the amplitude of vertical displacement and pitch angle decrease, and the amplitude of the roll angle increases. For example, the vertical displacement amplitude, by changing the electric current from zero *Amp* to 1.6 *Amp*, decreases in the peak point for profiles, speed bump 43%, sinusoidal harmonic 49%, and in the RMS value, for bump profiles 33 %, Sinusoidal harmonic% 59%, and random 10% decrease.

Table 4: Numerical results of simulation of secondary suspension mass center response in different electric currents and road profiles

Profile road	Current(A)	Peak value			RMS value		
		$z_{ss}(m)$	$\theta_{ss}(rad)$	$\varphi_{ss}(rad)$	$z_{ss}(m)$	$\theta_{ss}(rad)$	$\varphi_{ss}(rad)$
Harmonic	0	0.107	0.112	0.028	0.056	0.055	0.01
	0.5	0.07	0.103	0.042	0.046	0.06	0.16
	1.6	0.054	0.128	0.085	0.023	0.078	0.036
Speed Bump	0	0.16	0.029	0.034	0.058	0.018	0.016
	0.5	0.123	0.027	0..051	0.052	0.014	0.027
	1.6	0.091	0.016	0.121	0.043	0.012	0.064
Random	0	-	-	-	0.12	0.0004	0.039
	0.5	-	-	-	0.114	0.0003	0.055
	1.6	-	-	-	0.108	0.0002	0.08

4.2. Effect of irregular mass distribution of cargo on the secondary suspension system performance

The distribution of cargo in freight vehicles usually varies depending on the type of cargo. Therefore, this section examines the ability of the secondary magnetorheological suspension system to reduce the range of displacements caused by various road roughness at the center of mass of the sensitive cargo in different symmetrical and unsymmetrical distribution conditions of the sensitive cargo. To evaluate the performance of the secondary suspension system in this case, the different arrangements of the sensitive cargo according to Fig. 6a by using a 1200kg mass, m5, at the center of the secondary suspension plate (co-centered with the secondary suspension chassis) and a mass of 400kg, m3, at the pallet front on the co-driver's side and the 700kg mass, m4, on the driver's side at the rear of the pallet are created in three different mass distributions as below. These total cargo mass plus the mass of the pallet chassis (see Table 3) is 2621kg which is approximately in the middle range of the target payload mass(2000-3500kg) considered in designing four MR dampers for the secondary system.

A. All masses are equal to 2300kg together on the loaded pallet of the vehicle, so the layout has an uneven mass distribution over the longitudinal and transverse axis of the cargo and the truck.

B. By removing the 700kg mass from configuration A, it creates a more unbalanced mass distribution mode about the longitudinal and transverse axes of the sensitive cargo, with the total mass of the sensitive cargo equal to 1600kg.

C. By removing the 400kg and 700kg masses from configuration A, the balanced load distribution of the sensitive cargo will be equal to 1200kg.

All simulations are performed with a constant electric current of 0.6 Amp which is applied to all dampers simultaneously. The achieved results are summarized in Table 5. As a sample, the results of the simulation of the effect of the harmonic input were obtained using the three deferent mass distributions in directions of vertical and pith degrees of freedom of the center of mass of the secondary suspension system, which are presented in Fig. 10. Investigating the

results of different balanced and unbalanced mass distributions of sensitive cargo on the secondary magnetorheological suspension in different road profiles, the amplitude of the vertical displacement and pitch angle of the center of mass of the freight over the secondary suspension system changes as follows:

1. The vertical displacement amplitude in all three road profiles decreases with a decrease in the mass of the cargo over the secondary suspension system, with the peak point decreasing by 5% for speedbump input and 22% for the harmonic wave road surface. The RMS value of the vertical displacement curve also decreases by reducing the cargo mass from 2300 kg to 1200 kg at the speed bump input 12%, harmonic input 15.6% and the random input of 8%.
2. The RMS values of pitch angles in harmonic and speed bump road profiles by reducing cargo mass from 2300kg to 1600kg are associated with a 70% decrease meanwhile, by reducing cargo from 1600kg to 1200kg, this does not change much.

4.3. Transmissibility performance of the investigated secondary suspension system

In this section, we investigate the effect of MR dampers on transmissibility characteristics of the secondary suspension system, i.e., TR (ratio of the vertical displacement amplitude of the center of mass of the secondary suspension to the speedbump amplitude) at 0, 0.6, and 1.6$Amps$ simulated electric currents. Fig. 11 shows the TR graph of the center of mass displacement in the vertical direction of the secondary suspension system with magnetorheological dampers at different electric currents. As can be seen, with increasing electric current, the peak values of TR in the amplification region are decreased considerably, which is in agreement with the results obtained from the vertical displacement amplitude curves at the harmonic and speedbump inputs. According to the MR damper's TR curves, it is observed that as the electric current intensity increases, the secondary suspension isolation quality still is comparable to the off-state situation. Finally, it can be concluded that the secondary magnetorheological suspension system was successful in considerably reducing the peak amplitude of induced motions and at the same time providing good isolation characteristics.

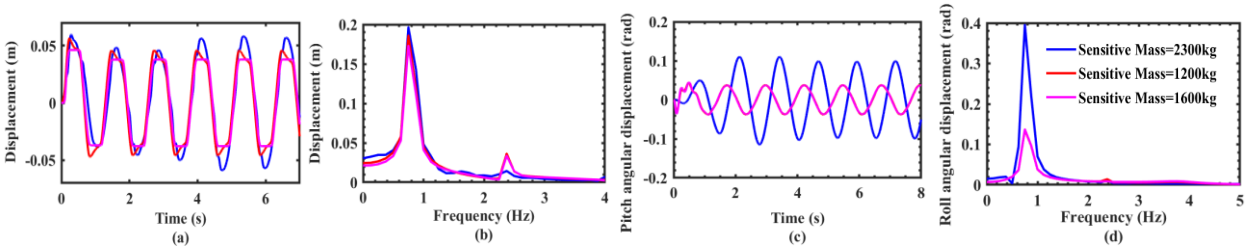

Fig 10: Time and frequency responses of payload's center of mass with a harmonic profile in 0.6 Amp respectively: (a) and (b), Vertical displacement, (c) and (d), Pitch angular displacement

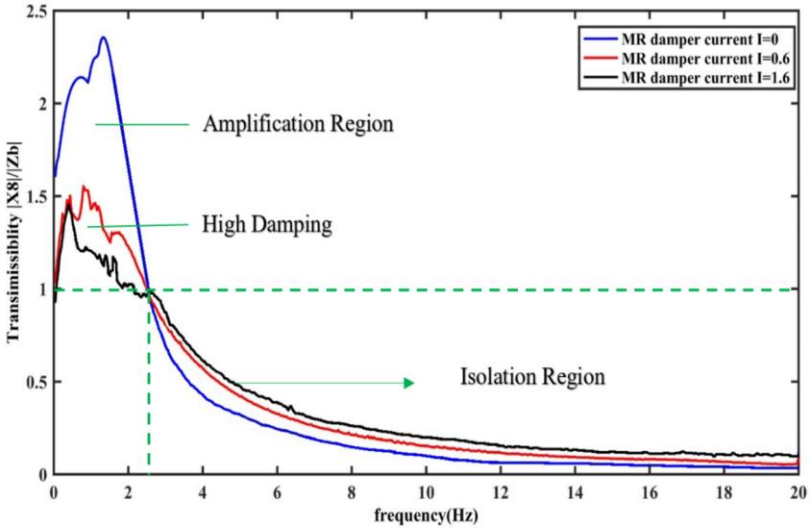

Fig 11: Transmissibility graphs and isolation regions of the vertical displacement of center of mass of the secondary suspension system with magnetorheological dampers at different electric currents

Table 5: Numerical results of the simulation of the response of the secondary magnetorheological suspension center of mass at different cargo masses and road profiles

Profile road	Sprung mass(Kg)	Peak value		RMS value	
		$z_{ss}(m)$	$\theta_{ss}(rad)$	$z_{ss}(m)$	$\theta_{ss}(rad)$
Harmonic	2300	0.059	0.011	0.032	0.068
	1600	0.056	0.044	0.03	0.025
	1200	0.046	0.044	0.027	0.025
Speed Bump	2300	0.125	0.033	0.055	0.034
	1600	0.125	0.075	0.051	0.025
	1200	0.119	0.075	0.048	0.025
Random	2300	-	-	0.119	0.002
	1600	-	-	0.114	0.006
	1200	-	-	0109	0.009

5. Conclusion

In this study, a double-ended magnetorheological damper was modeled and prototyped for use in the secondary cargo suspension system and evaluated by dynamic tests on a UTM test machine. Dynamic test results of the damper indicate that this damper is suitable to produce enough dissipative force for use in secondary suspension systems in light trucks to protect sensitive cargoes. Using the results of UTM test, the parameters of the Modified Bouc-Wen parametric model for the magnetorheological damper were identified and applied to update the model of the considered secondary suspension system.

Using the updated model of truck containing secondary magnetorheological suspension system, the effects of irregular arrangement of cargoes and different electrical currents on the secondary suspension were analyzed, while different road profiles the considered in simulations. The vertical displacement amplitude of the center of mass of cargo laying over the secondary magnetorheological suspension in all considered road profiles i.e., harmonic wave, random, and speedbump has been reduced by an average of 40% at Peak point and a 30% decrease in RMS value by increasing the electric current of the magnetorheological damper from 0-1.6Amp. By decreasing the mass of the cargo arranged irregularly, the vertical displacement amplitude of the center of mass of the secondary magnetorheological suspension model is reduced in all three road profiles so that the peak point in the speedbump inputs 5% and the harmonics 22% is reduced. The RMS value of the vertical displacement curve also decreased by reducing the cargo mass from 2300 kg to 1200 kg, 12% at speedbump input,15.6% at harmonic wave input, and 8% at random input, which means that the magnetorheological damper performance is good at reducing vibrations in the vertical direction.

Based on the achieved results, it can be concluded that the introduced secondary magnetorheological suspension system for sensitive cargo under various conditions of road roughness for uneven distribution of sensitive cargo mass was able to reduce the vertical displacement and, in most cases, the pitch angle amplitudes and provided acceptable isolation region behavior. Making a laboratory-scale sensitive payload prototype pallet using the MR dampers similar to the prototype designed and fabricated in this study, installing it on a light truck and doing road tests with standard road obstacles such as speed bumps is the next step to complete this work. Furthermore, developing an appropriate controlling strategy based on online recognition of the road surface obstacles in front of the moving truck will be the other necessary aim of the future research.

Conflict of interest On behalf of all authors, the corresponding author states that there is no conflict of interest.

Appendix

The relations for $Y_{t1} - Y_{t4}$ and $Y_{P1} - Y_{P4}$ that were used in equations (14)-(23) are presented as following:

$$Y_{t1} = \left(-\dot{z}_{l1} + \dot{z}_{fs} + a_2\dot{\theta}_{fs} - b_2\dot{\varphi}_{fs}\right) \tag{30}$$

$$Y_{t2} = \left(-\dot{z}_{l2} + \dot{z}_{fs} - a_1\dot{\theta}_{fs} - b_2\dot{\varphi}_{fs}\right) \tag{31}$$

$$Y_{t3} = \left(-\dot{z}_{r1} + \dot{z}_{fs} + a_2\dot{\theta}_{fs} + b_1\dot{\varphi}_{fs}\right) \tag{32}$$

$$Y_{t4} = \left(-\dot{z}_{r2} + \dot{z}_{fs} - a_1\dot{\theta}_{fs} + b_1\dot{\varphi}_{fs}\right) \tag{33}$$

$$Y_{p1} = \left(z_{ss} - z_{fs} + a_6\left(\theta_{ss} - \frac{a_4 + a_3}{a_6 + a_5}\theta_{fs}\right) - b_6\left(\varphi_{ss} - \frac{b_4 + b_3}{b_5 + b_6}\varphi_{fs}\right)\right) \tag{34}$$

$$Y_{p2} = \left(z_{ss} - z_{fs} - a_5\left(\theta_{ss} - \frac{a_4 + a_3}{a_6 + a_5}\theta_{fs}\right) - b_6\left(\varphi_{ss} - \frac{b_4 + b_3}{b_5 + b_6}\varphi_{fs}\right)\right) \tag{35}$$

$$Y_{p3} = \left(z_{ss} - z_{fs} + a_6\left(\theta_{ss} - \frac{a_4 + a_3}{a_6 + a_5}\theta_{fs}\right) + b_5\left(\varphi_{ss} - \frac{b_4 + b_3}{b_5 + b_6}\varphi_{fs}\right)\right) \tag{36}$$

$$Y_{p4} = \left(z_{ss} - z_{fs} - a_5\left(\theta_{ss} - \frac{a_4 + a_3}{a_6 + a_5}\theta_{fs}\right) + b_5\left(\varphi_{ss} - \frac{b_4 + b_3}{b_5 + b_6}\varphi_{fs}\right)\right) \tag{37}$$

References

[1] F. Queslati, S. Sankar, Performance of a fail-safe active suspension with limited state feedback for improved ride quality and reduced pavement loading in heavy vehicles, SAE transactions, (1992) 796-804.
[2] K. Jahani, M. Dehnad, Identifying the frequency dependent material property of a hydraulic engine mount through an iterative procedure using 3D finite element modeling, Journal of Mechanical Science and Technology, 28 (2014) 2041-2047.
[3] C. Ekberg, E. Hansson, Design and simulation of active and semi-active cab suspensions with focus to improve ride comfort of a heavy truck, in, 2015.
[4] L. Zhao, C. Zhou, Y. Yu, Hybrid modeling of seat-cab coupled system for truck, International Journal of Automotive Technology, 17 (2016) 769-776.
[5] S.-H. Kim, D.-S. Yoon, G.-W. Kim, S.-B. Choi, J.-Y. Jeong, J.-H. Kim, S.-J. Kim, I.-D. Kim, Road traveling test for vibration control of a wheel loader cabin installed with magnetorheological mounts, Journal of Intelligent Material Systems and Structures, 32 (2021) 1336-1348.
[6] B.D. Van Deusen, Truck suspension system optimization, SAE Transactions, (1971) 886-896.
[7] L. Balamurugan, J. Jancirani, M. Eltantawie, Generalized magnetorheological (MR) damper model and its application in semi-active control of vehicle suspension system, International Journal of Automotive Technology, 15 (2014) 419-427.
[8] D. Fischer, M. Börner, R. Isermann, Control of mechatronic semi-active vehicle suspensions, IFAC Proceedings Volumes, 35 (2002) 209-214.
[9] F.M. Marcu, Semiactive Cab Suspension control for semitruck applications, in, Virginia Tech, 2009.
[10] H.D. Chae, S.-B. Choi, A new vibration isolation bed stage with magnetorheological dampers for ambulance vehicles, Smart Materials and Structures, 24 (2014) 017001.
[11] M. Mao, W. Hu, Y.-T. Choi, N.M. Wereley, A magnetorheological damper with bifold valves for shock and vibration mitigation, Journal of Intelligent Material Systems and Structures, 18 (2007) 1227-1232.
[12] S. Sun, D. Ning, J. Yang, H. Du, S. Zhang, W. Li, A seat suspension with a rotary magnetorheological damper for heavy duty vehicles, Smart Materials and Structures, 25 (2016) 105032.
[13] Q. Wang, M. Ahmadian, Z. Chen, A novel double-piston magnetorheological damper for space truss structures vibration suppression, Shock and Vibration, 2014 (2014).
[14] G. Yang, Large-scale magnetorheological fluid damper for vibration mitigation: modeling, testing and control, University of Notre Dame, 2002.
[15] Y.-f. Zhou, H.-l. Chen, Study on damping properties of magnetorheological damper, Frontiers of Mechanical Engineering in China, 1 (2006) 452-455.
[16] R.M. Desai, M.E.H. Jamadar, H. Kumar, S. Joladarashi, S. Raja Sekaran, Design and experimental characterization of a twin-tube MR damper for a passenger van, Journal of the Brazilian Society of Mechanical Sciences and Engineering, 41 (2019) 1-21.

[17] X. Zhao-Dong, J. Da-Huan, Z. Xiang-Cheng, Performance tests and mathematical model considering magnetic saturation for magnetorheological damper, Journal of Intelligent Material Systems and structures, 23 (2012) 1331-1349.
[18] G. Yang, B.F. Spencer Jr, H.-J. Jung, J.D. Carlson, Dynamic modeling of large-scale magnetorheological damper systems for civil engineering applications, Journal of Engineering Mechanics, 130 (2004) 1107-1114.
[19] N. Kwok, Q. Ha, M. Nguyen, J. Li, B. Samali, Bouc–Wen model parameter identification for a MR fluid damper using computationally efficient GA, ISA transactions, 46 (2007) 167-179.
[20] Y. Peng, J. Yang, J. Li, Parameter identification of modified Bouc–Wen model and analysis of size effect of magnetorheological dampers, Journal of Intelligent Material Systems and Structures, 29 (2018) 1464-1480.
[21] Q. Sun, L. Zhang, J. Zhou, Q. Shi, Experimental study of the semi-active control of building structures using the shaking table, Earthquake engineering & structural dynamics, 32 (2003) 2353-2376.
[22] B. Spencer Jr, S. Dyke, M. Sain, J. Carlson, Phenomenological model for magnetorheological dampers, Journal of engineering mechanics, 123 (1997) 230-238.
[23] S.-B. Choi, M.-H. Nam, B.-K. Lee, Vibration control of a MR seat damper for commercial vehicles, Journal of intelligent material systems and structures, 11 (2000) 936-944.
[24] A. Heidarian, X. Wang, Review on seat suspension system technology development, Applied Sciences, 9 (2019) 2834.
[25] F. Yang, L. Zhao, Y. Yu, C. Zhou, Matching, stability, and vibration analysis of nonlinear suspension system for truck cabs, Shock and Vibration, 2019 (2019).
[26] M. Mousazadeh, K. Jahani, S.S. Samadani Aghdam, Experimental Study of the Effects of Iron Particles Size on Damping Force and Energy Dissipation of a Double-Ended Magnetorheological Damper, Modares Mechanical Engineering, 19 (2019) 2129-2138.
[27] H.J. Singh, N.M. Wereley, Optimal control of gun recoil in direct fire using magnetorheological absorbers, Smart materials and Structures, 23 (2014) 055009.
[28] M. Yu, C. Liao, W. Chen, S. Huang, Study on MR semi-active suspension system and its road testing, Journal of intelligent material systems and structures, 17 (2006) 801-806.
[29] M. Mao, W. Hu, Y.T. Choi, N. Wereley, A.L. Browne, J. Ulicny, Experimental validation of a magnetorheological energy absorber design analysis, Journal of Intelligent Material Systems and Structures, 25 (2014) 352-363.
[30] F. White, M., 1986, Fluid Mechanics, in, Mc Graw Hill Book Company, New York, 1979.
[31] M. Dassisti, G. Brunetti, Introduction to Magnetorheological Fluids, (2022).
[32] J. de Vicente, F. Vereda, J.P. Segovia-Gutiérrez, M. del Puerto Morales, R. Hidalgo-Álvarez, Effect of particle shape in magnetorheology, Journal of Rheology, 54 (2010) 1337-1362.
[33] D. Wang, W.H. Liao, Magnetorheological fluid dampers: a review of parametric modelling, Smart materials and structures, 20 (2011) 023001.
[34] E. Yarali, A. Mohammadi, S. Mafakheri, M. Baghani, H. Adibi, Mathematical modeling and experimental evaluation of a prototype double-tube Magnetorheological damper, SN Applied Sciences, 1 (2019) 1-10.
[35] T.D. Gillespie, S.M. Karamihas, Simplified models for truck dynamic response to road inputs, International Journal of Heavy Vehicle Systems, 7 (2000) 52-63.
[36] in https://www.isuzu.com.au/Media/Isuzu_Files/Spec_Sheets/Current_spec_sheets/NPR%2075-190%20CREW_ARK1350_v02.pdf .
[37] M. Agostinacchio, D. Ciampa, S. Olita, The vibrations induced by surface irregularities in road pavements–a Matlab® approach, European Transport Research Review, 6 (2014) 267-275.